Robo and Ror function in a common receptor complex to regulate Wnt-mediated neurite outgrowth in *Caenorhabditis elegans*

Jiaming Wang[a,b] and Mei Ding[a,c,1]

[a]State Key Laboratory of Molecular Developmental Biology, Institute of Genetics and Developmental Biology, Chinese Academy of Sciences, 100101 Beijing, China; [b]Biological Science Department, University of Chinese Academy of Sciences, 100049 Beijing, China; and [c]Center for Excellence in Brain Science and Intelligence Technology, Chinese Academy of Sciences, Beijing 100101, China

Edited by Gian Garriga, University of California, Berkeley, CA, and accepted by Editorial Board Member Roeland Nusse January 30, 2018 (received for review October 10, 2017)

Growing axons are exposed to various guidance cues en route to their targets, but the mechanisms that govern the response of growth cones to combinations of signals remain largely elusive. Here, we found that the sole Robo receptor, SAX-3, in *Caenorhabditis elegans* functions as a coreceptor for Wnt/CWN-2 molecules. SAX-3 binds to Wnt/CWN-2 and facilitates the membrane recruitment of CWN-2. SAX-3 forms a complex with the Ror/CAM-1 receptor and its downstream effector Dsh/DSH-1, promoting signal transduction from Wnt to Dsh. *sax-3* functions in Wnt-responsive cells and the SAX-3 receptor is restricted to the side of the cell from which the neurite is extended. DSH-1 has a similar asymmetric distribution, which is disrupted by *sax-3* mutation. Taking these results together, we propose that Robo receptor can function as a Wnt coreceptor to regulate Wnt-mediated biological processes in vivo.

Wnt | Robo receptor | Ror receptor | Dsh | PCP

When axons navigate through a complex in vivo environment, at any given point they are probably confronted with several different guidance cues. Given the large number of different axon trajectories, it remains an enduring mystery how wiring specificity is achieved by a limited repertoire of secreted molecules. Accumulating evidence from a variety of model systems in the past decades has revealed several strategies that evolution may take to solve this problem. Among them, the combinatorial use of different wiring molecules has been considered an efficient way to reduce the overall number of molecules needed. For example, expression of deleted in colon cancer (DCC) alone produces an attractive response to netrin, whereas coexpression of DCC with Unc5 (uncoordinated) produces a repulsive response to the same guidance cues (1, 2). Noticeably, combinatorial usage occurs among different cue-receptor pairs. Commissural axons use DCC and Robo as receptors to respond to netrin and Slit, respectively. Before an axon crosses the midline, the attractive signaling of netrin-DCC is dominant over the repulsive signaling of Slit-Robo. Once an axon reaches the midline, however, activation of Robo silences the netrin-DCC–mediated attraction through direct binding of Robo to DCC (3). Apparently, the above processes guide axons with remarkable precision along their complex journey, but how these guidance molecules interact in space and time to pattern complex nervous systems is not fully understood.

Robos are widely recognized as repulsive receptors for Slit ligands (4–6). However, a recent study showed that Robo3 also binds to neural epidermal growth factor-like-like 2 (NELL2) and axons carrying Robo3 are repelled by NELL2 (7). Unlike Robo1 or Robo2, the Robo3 receptor appears not to bind to Slit (8–11). Intriguingly, recent studies demonstrated that Robo3 can signal through the DCC receptor, which is responsive to Netrin (10). In *Caenorhabditis elegans*, the sole Robo (SAX-3) has a profound effect on nervous system development (12–14). In contrast, loss-of-function of the only Slit (SLT-1) has a rather mild effect and the nerve ring organization appears normal, suggesting that the Robo receptor may also respond to other cues.

Wnts are secreted extracellular molecules that act through a number of distinct signaling pathways to regulate a variety of biological processes. Canonical Wnt signaling is activated by Wnt binding to the Frizzled receptor (Frz) and LDL-receptor–related protein families, which triggers nuclear translocation of β-catenin to regulate transcription of specific target genes (15). The kinase-like orphan receptor (Ror) proteins can also serve as Wnt receptors signaling via novel noncanonical Wnt pathways and have been implicated in neuronal migration, neurite outgrowth, axon guidance, axonal pruning, axonal branching, and synapse formation (16–22).

Here, we found that instead of mediating Slit signaling, the Robo receptor binds and responds to Wnt to promote directional neurite outgrowth in *C. elegans*. By forming a complex with the Ror receptor and Dsh effector, Robo promotes signal transduction from Wnt to Dsh. Taken together, our results reveal a mechanistic link between Robo receptor and Wnt-Ror-Dsh signaling.

Results

Robo/SAX-3 Receptor Associates with Ror/CAM-1 Receptor. The RME neurons are a set of four GABAergic motor neurons that innervate head muscles and regulate foraging movements in *C. elegans* (23). Among them, RMEL and RMER only send out

Significance

How a limited repertoire of secreted molecules pattern a large number of axon trajectories is an enduring mystery. Both Slit-Robo and Wnt-Ror pathways are involved in proper neurite extension, but whether and how these two signaling pathways are interacted is largely unknown. Here, we found that instead of mediating Slit signaling, Robo could bind and respond to Wnt ligand. By forming a complex with the Ror receptor and Dsh effector, the Robo receptor promotes signal transduction from Wnt to Dsh. The mechanistic link between the Robo receptor and Wnt-Ror-Dsh signaling revealed here will markedly advance our understanding of how guidance molecules interact in space and time to orchestrate the dynamic process of growth cone navigation through a complex cellular environment.

Author contributions: J.W. and M.D. designed research; J.W. performed research; J.W. and M.D. analyzed data; and J.W. and M.D. wrote the paper.

The authors declare no conflict of interest.

This article is a PNAS Direct Submission. G.G. is a guest editor invited by the Editorial Board.

[1]To whom correspondence should be addressed. Email: mding@genetics.ac.cn.

This article contains supporting information online at www.pnas.org/lookup/suppl/doi:10.1073/pnas.1717468115/-/DCSupplemental.

Published online February 20, 2018.

processes to the nerve ring region. In contrast, RMED and RMEV each send out an extra process, which runs down the dorsal and ventral cords, respectively, and then terminates around the middle of the body (Fig. 1*A*) (24). Using a GFP transgene driven by the GABAergic neuron-specific promoter *Punc-25*, we were able to visualize the morphology of RME neurons in *unc-30* mutant animals (Fig. S1 *A* and *B*). *unc-30* encodes a homeodomain protein that controls the specification of type D GABA neurons. In the absence of UNC-30, *unc-25* expression in type D neurons is abolished; however, its expression remains unchanged in RME neurons. Therefore, using the *Punc-25*::GFP marker in the *unc-30* mutant background, we were able to specifically follow the development of RME neurons in living animals at the single-cell level (Fig. 1*B*).

We previously reported that the Ror/CAM-1 receptor acts on RMED/V cells and transmits the CWN-2 signal, probably through direct association, to Dsh/DSH-1 to regulate the posterior neurite growth of RMED/V (17). In animals carrying the full loss-of-function alleles *cam-1(gm122)* or *dsh-1(ok1445)*, the neurites of RMED/V cells are very short or absent (17) (Fig. 1 *C* and *D* and Fig. S1 *C* and *D*). Intriguingly, the *cam-1(ks52)* and *cam-1(gm105)* mutations, which disrupt the intracellular domain of CAM-1 (Fig. 1*C* and Fig. S1 *E*–*G*), cause a distinctive short RMED/V neurite phenotype, which is weaker than the *cam-1* null (Fig. 1*D* and Fig. S1 *C* and *D*). This suggests that other receptor components are necessary to facilitate transmission of the Wnt/CWN-2 signal by CAM-1 to DSH-1. Hence, we performed a yeast two-hybrid screen using the CAM-1 intracellular domain (ICD) as a bait and identified the Robo/SAX-3 receptor (Fig. S2*A*). Additional coimmunoprecipitation (co-IP) assays confirmed that the SAX-3 protein indeed associates with CAM-1 ICD (Fig. 1*E*).

SAX-3 Functions with CAM-1 Receptor to Regulate Neurite Outgrowth. Next, we tested whether *sax-3* plays a role in RMED/V neurite outgrowth similar to *cam-1*. The *sax-3(ky123)* allele deletes the first exon of *sax-3*, which results in an ORF shift that covers the whole *sax-3* gene and is likely a molecular null. *sax-3(ky203)* contains a nonsense mutation immediately after the transmembrane domain. In *sax-3(ky123)* and *sax-3(ky203)* mutant animals, we found that the neurite length of both RMED and RMEV is significantly reduced (Fig. 1 *F*–*H*). The defect in *sax-3(ky203)*

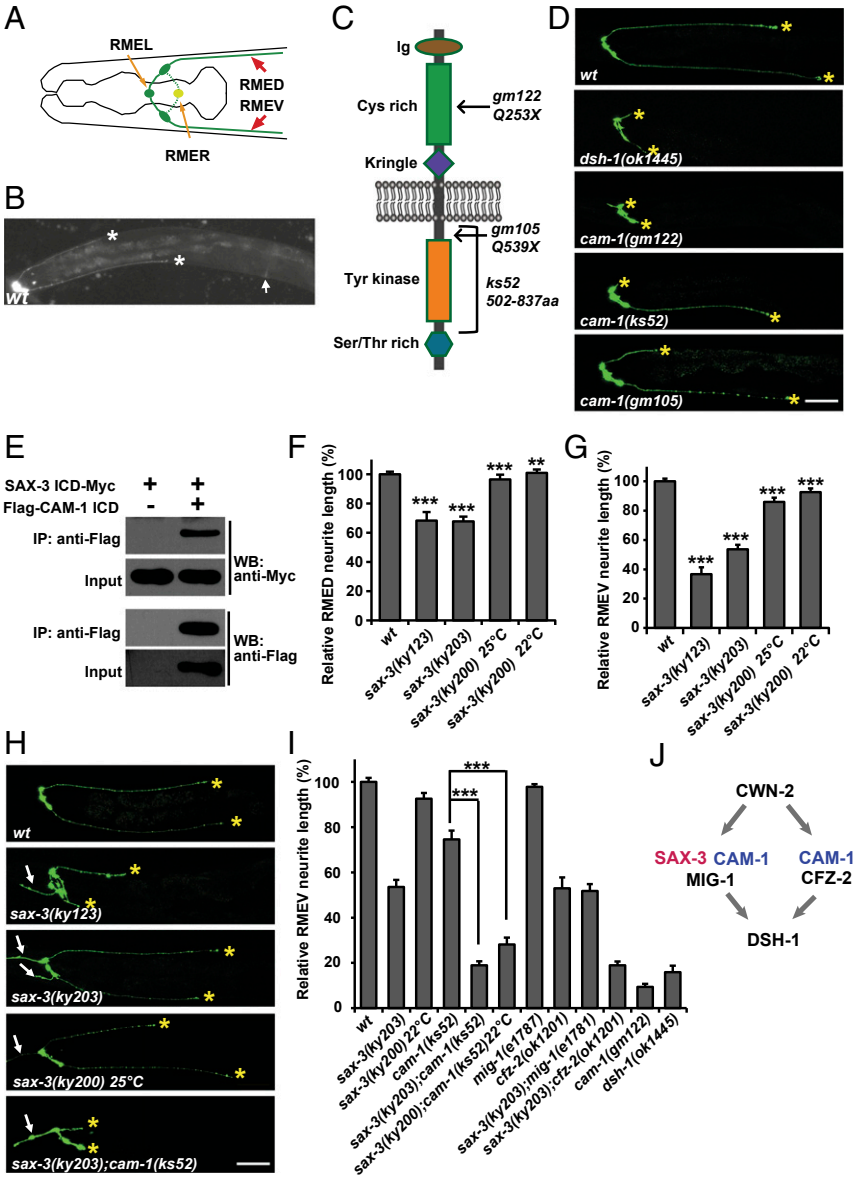

Fig. 1. SAX-3 participates in RMED/V neurite outgrowth. (*A*) Schematic drawing of all four RME neurons. Anterior is to the left and dorsal is up. (*B*) A GFP fluorescence image of RME neurons, obtained by expressing *Punc-25*::GFP in the *unc-30* mutant background. White asterisks indicate the tips of RMED/V neurites. Arrow marks the vulva region. (*C*) Schematic drawing of the protein structure of the CAM-1 receptor. The molecular lesions in *gm122*, *gm105* and *ks52* are indicated. (*D*) Representative images of RMED/V posterior neurites. Yellow asterisks indicate the tips of RMED/V neurites. (Scale bar, 50 μm.) (*E*) Myc-tagged SAX-3 ICD binds to Flag-tagged CAM-1 ICD in coprecipitation assays. (*F* and *G*) Quantification of the neurite outgrowth defect in *sax-3* mutant animals. $n \geq 50$ for each genotype; $^{***}P < 0.001$; $^{**}P < 0.01$. One-way ANOVA with Dunnett's test. (*H*) RMED/V neurite outgrowth in *sax-3* mutants. (*I*) Quantification of the RMEV neurite length in various genotypes. Data are expressed as mean ± SEM; $n \geq 50$ for each genotype; $^{***}P < 0.001$; NS, not significant. One-way ANOVA with Bonferroni's test. (*J*) Genetic interaction between different Wnt receptors.

mutants is almost as severe as in *sax-3(ky123)* mutants (Fig. 1 *F* and *G*), suggesting that *sax-3(ky203)* probably acts as a null or strong loss-of-function allele in neurite outgrowth. The temperature-sensitive allele *sax-3(ky200)* shows a weak neurite outgrowth defect at the restrictive temperature (25 °C), which is marginally alleviated when animals are cultivated at a more permissive temperature (22 °C) (Fig. 1 *F* and *G*). Thus, *sax-3* is indeed involved in RMED/V neurite outgrowth.

The association between SAX-3 and the cytoplasmic domain of CAM-1 hinted that Robo/SAX-3 may function with the CAM-1 receptor. If this is the case, we would expect that the loss of SAX-3 function would worsen the short neurite defect of *cam-1* mutants, particularly those that lack the intracellular domain of CAM-1. Hence, we created double mutants between *sax-3(ky203)* and *cam-1(ks52)*. In these double-mutant animals, the posterior neurite extension of RMED/V is completely blocked, suggesting a complete signaling transduction failure from CWN-2 to DSH-1 (Fig. 1*I* and Fig. S2*B*). We further created *cam-1(ks52);sax-3 (ky200)* doubles and found that the outgrowth of the posterior neurites of RMED/V neurites is also completely blocked (Fig. 1*I* and Fig. S2*B*). The observation that double mutants carrying an intracellular null of *cam-1* with a *sax-3* null resemble single mutants with full loss-of-function of *cam-1* raises the possibility that Robo/SAX-3 receptor cooperates with CAM-1 to transduce the Wnt signal to the cytosol. Our attempt to make double mutants of the *cam-1(gm122)* null with *sax-3(ky203)* or *sax-3(ky123)* was unsuccessful, suggesting a strong lethality. Indeed, when we constructed *cam-1(gm122);sax-3(ky203)* double animals with the wild-type *sax-3* gene expressed extrachromosomally, we found that their progeny were arrested at the early larval stage. Given the fact that none of those dead larvae carried the wild-type *sax-3* gene, we believe that they were *cam-1(gm122);sax-3(ky203)* doubles. The strong lethality of *cam-1(null);sax-3(null)* suggests that Ror/CAM-1 and Robo/SAX-3 may function together in other developmental processes as well (Fig. S2 *C* and *D*) (25).

The classic Frz receptors MIG-1 and CFZ-2 are also involved in RMED/V neurite outgrowth (17). Compared with *cam-1*, null mutants of *cfz-2* or *mig-1* only display mild neurite outgrowth defects (Fig. 1*I* and Fig. S2*B*). In addition, *mig-1;cfz-2* double mutants exhibit a more severe phenotype resembling *cam-1* null (17), which suggests that CFZ-2 and MIG-1 function redundantly. When both SAX-3 and CFZ-2 receptors are removed, we found that the RMED/V neurite length is much shorter than in either *sax-3*– or *cfz-2*–null mutants (Fig. 1*I* and Fig. S2*B*), suggesting a redundant interaction between these two genes. The neurite length in *sax-3(ky203);mig-1(e1787)* animals is similar to that in *sax-3(ky203)* single mutants (Fig. 1*I* and Fig. S2*B*), suggesting that *mig-1* may function in the same pathway as *sax-3* (Fig. 1*J*).

In addition to the shorter posterior neurite, ectopic anterior neurites are observed in *sax-3* mutant animals (Fig. 1*H*, white arrows). Additonal phenotypic analysis showed that those ectopic anterior neurites are mainly derived from RMEL and RMER neurons and their growth is likely independent of Wnt-Ror-Dsh signaling (Fig. S2 *E* and *F*).

***Sax-3* Acts Cell-Autonomously.** A GFP construct driven by a 4-kb *sax-3* promoter revealed a wide *sax-3* expression pattern in the nervous system (Fig. 2*A* and Fig. S3 *A* and *B*). The protein-coding region of *sax-3* driven by this promoter fully restored the neurite length to wild-type level, suggesting that the expression pattern revealed by this promoter represents the endogenous *sax-3* distribution (Fig. 2 *B* and *C*). To identify whether *sax-3* is expressed in RMED/V neurons, we specifically highlighted the RME neurons with *Punc-25*::mCherry in the *unc-30* mutant background and found that *Psax-3*::GFP is present in both RMED and RMEV neurons (Fig. S3*B*). Furthermore, we introduced nuclear localization sequence (NLS)-tagged GFP driven by *Psax-3* into worms. As shown in Fig. 2*A*, double labeling with *Punc-25*::mCherry in *unc-30* mutants revealed that the *sax-3* gene is indeed expressed in both RMED and RMEV neurons. We then tested whether *sax-3* functions in Wnt/CWN-2–responsive cells (RMED/V). When a wild-type copy of *sax-3* was expressed in the whole nervous system using the pan-neuronal promoter P*snb-1*, we found that the short posterior neurite outgrowth defects were efficiently rescued (Fig. 2 *B* and *C*). *cam-1* is expressed in a subset of neurons including RMED/V (17). The significant rescuing activity of a *sax-3* construct driven by the P*cam-1b* promoter indicated that *sax-3* can function in *cam-1*–expressing cells (Fig. 2 *B* and *C*). In *unc-30* mutants, the P*unc-25* promoter drives gene expression, specifically in RME neurons. With this approach, we examined whether expressing *sax-3* only in RME cells was able to restore the RMED/V neurite length. Indeed, we found that the shortened RMED/V neurite phenotype was significantly rescued (Fig. 2 *B* and *C*). *unc-47* encodes the GABA transporter in *C. elegans*. In the absence of the UNC-30 homeodomain protein, *unc-47* gene expression is also restricted in RME neurons in the nerve ring region. When *sax-3* was expressed in *unc-30* mutant worms using the P*unc-47* promoter, significant rescue activity was observed (Fig. 2 *B* and *C*). Thus, *sax-3* can function cell-autonomously within RME cells to regulate neurite outgrowth. We additionally created a tissue-specific knockout of *sax-3* in RME cells using the P*unc-25* promoter to drive the CRISPR/Cas9 system (Fig. S3 *C* and *D*). We found that the RMEV neurite length is noticeably reduced compared with wild-type (Fig. S3*E*). Although on average the RMED neurite length is indistinguishable from wild-type, we did notice that some of the knockout animals display shorter RMED neurites (Fig. S3*F*). RME cells are born earlier than the onset of *unc-25* gene expression and the tissue-specific knockout efficiency with the current system is rather limited (26). The relatively weak (compared with *sax-3* mutant animals) neurite extension defect in those RME-specific *sax-3* knockout animals may due to the above limitations. In contrast, expression of the *sax-3* gene driven by the P*unc-86* promoter in neurons other than RME in the nerve ring did not rescue the short RMED/V neurite defect caused by *sax-3* mutation (Fig. 2 *B* and *C*). The P*hlh-17* promoter drives gene expression in glia-like sheath cells surrounding the nerve ring area. When we introduced *sax-3* gene expression into the sheath cells using the P*hlh-17* promoter, no rescue activity was observed (Fig. 2 *B* and *C*), suggesting that *sax-3* probably does not function on close-by neurons or tissues to regulate RMED/V neurite growth. Together, these results provide evidence that *sax-3* functions cell-autonomously within RME neurons to regulate neurite growth.

Slit/SLT-1 Is Not Involved in RMED/V Neurite Outgrowth. The classic ligands for Robo receptors are Slit proteins. We wondered whether Robo/SAX-3 responds to Slit to regulate RMED/V neurite growth. *C. elegans* has a single Slit ligand, SLT-1. In null *slt-1(eh15)* animals, no obvious neurite outgrowth defect was detected (Fig. 2 *D*–*F*). The *srgp-1* gene encodes the sole sr-GAP (Slit-Robo-GTPase activating protein), which is implicated in the Slit-Robo pathway (27–29). In animals carrying the loss-of-function allele *srgp-1(ok300)*, the RMED/V neurite length is indistinguishable from wild-type (Fig. 2 *D*–*F*). Hence, the typical Slit-Robo pathway appears not play a significant role in REMD/V neurite outgrowth.

Slit may function redundantly with the Wnt-Ror-Dsh pathway, in which case *slt-1* single mutants cannot reveal the functional requirement for Slit in RMED/V outgrowth. Elimination of the Wnt-Ror-Dsh pathway leads to complete blockage of RMED/V neurite growth. Thus, it is not feasible to reveal the redundant role of *slt-1* by making double mutants between *slt-1* and any of the *cwn-2*, *cam-1*, or *dsh-1* nulls. Nevertheless, we created the *slt-1(e15);cam-1(gm122)* double mutant and found that its phenotype resembles the null *cam-1(gm122)* (Fig. 2*D*). In contrast, the *cam-1(ks52)* mutation, which affects the intracellular domain of CAM-1, causes a partial outgrowth defect. Hence, we further created the *slt-1(e15);cam-1(ks52)* double mutant and found that

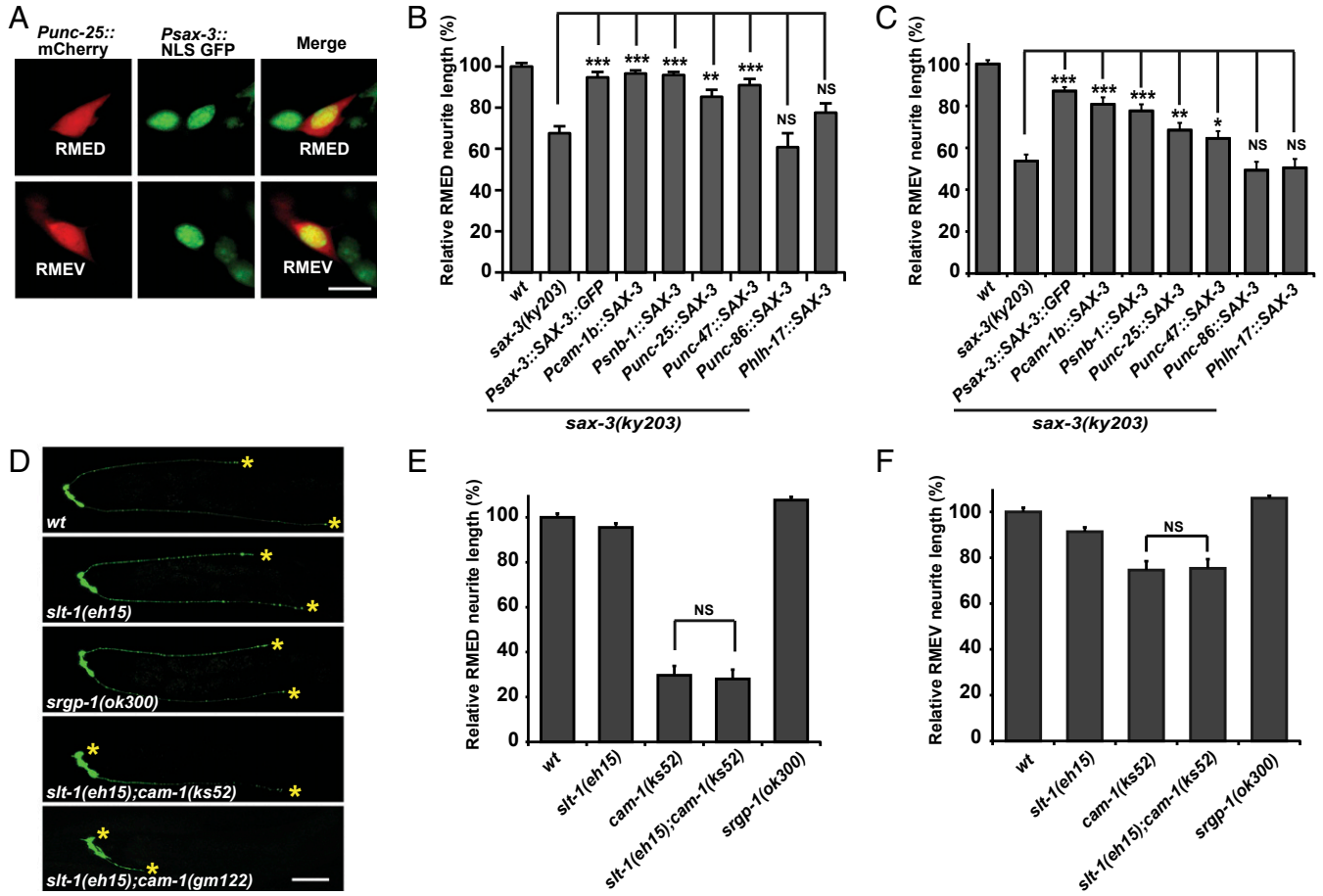

Fig. 2. SAX-3 functions cell-autonomously and independently from Slit. (*A*) Colocalization between *Psax-3*::NLS GFP (green) and P*unc-25*::*mCherry* (red). (Scale bar, 5 μm.) (*B* and *C*) Rescue of the RMED (*B*) and RMEV (*C*) neurite length by tissue-specific expression of *sax-3* using different promoters. $n \geq 50$ for each genotype; $***P < 0.001$; $**P = 0.004$; $*P = 0.04$; NS, not significant. One-way ANOVA with Dunnett's test. All phenotypes are scored in *unc-30* mutant background. (*D*) Representative images of RMED/V posterior neurites in different worms. Yellow asterisks indicate neurite tips. (Scale bar, 50 μm.) (*E* and *F*) Quantification of the RMED (*E*) and RMEV (*F*) neurite length. Data are expressed as mean ± SEM; $n \geq 50$ for each genotype; NS, not significant. One-way ANOVA with Fisher's least significant difference (LSD) test. (Scale bar, 50 μm.)

the neurite outgrowth defect is comparable to the *cam-1(ks52)* single mutant (Fig. 2 *D*–*F*). This suggests that the Slit ligand is not acting redundantly with the Wnt-Ror-Dsh pathway to regulate neurite outgrowth.

SAX-3 Binds to Wnt/CWN-2. The noninvolvement of Slit suggests that the Robo/SAX-3 receptor may sense other ligands to mediate neurite outgrowth. Given that SAX-3 associates with CAM-1 and CAM-1 functions as a CWN-2 receptor during RMED/V neurite extension, we suspected that SAX-3 may respond to the Wnt/CWN-2 ligand instead. To test this possibility, we constructed C-terminal Myc-tagged CWN-2 (CWN-2–Myc) to examine whether SAX-3 can bind to CWN-2. When introduced into *cwn-2(xd1)* mutant worms, this CWN-2–Myc-expressing construct significantly rescued the short neurite defect (Fig. S4 *A* and *B*), which suggests that the Myc tag does not affect CWN-2 function. We then coexpressed both CWN-2–Myc and SAX-3–Flag in HEK293T cells and performed co-IP tests. Considering that the SAX-3 receptor contains a transmembrane domain, we used Myri-GFP, a plasma membrane reporter, and the integral membrane protein connexin43 (CX43) as negative controls to eliminate the possibility that the membrane-anchoring feature of SAX-3 may be responsible for CWN-2 association. As shown in Fig. 3*A*, CWN-2–Myc was specifically coimmunoprecipitated with SAX-3–Flag but not with Myri-GFP or CX43. We further tested whether SAX-3 can directly bind to CWN-2 using GST pull-down assays. After affinity purification, the CWN-2–GST and SAX-3–Flag proteins were incubated together and the pull-down experiments were performed. We found that CWN-2–GST, but not GST alone, pulled down SAX-3–Flag (Fig. 3*B*).

We further divided SAX-3 into the ectodomain (ECD) and ICD and found that only full-length SAX-3 and the ECD bound with CWN-2 (Fig. 3*C*). SAX-3 ECD contains five Ig domains and three fibronectin domains. From structure-function analysis, we found that the Ig1 domain and the fibronectin domains of SAX-3 were both capable of interacting with CWN-2 (Fig. 3*D*). We additionally tested the CWN-2–binding activity of individual fibronectin repeats and identified that both the second and third fibronectin domains possess the ability to bind to CWN-2 (Fig. 3*E*).

SAX-3 Facilitates the Membrane Recruitment of CWN-2. How does CWN-2–SAX-3 interaction affect CWN-2 signaling through the CAM-1 receptor? CAM-1 has been implicated in Wnt binding previously (30). Indeed, Flag-tagged CAM-1 receptor associated with functional CWN-2–Myc in a co-IP assay (Fig. 4*A*). When a similar amount of SAX-3 or CAM-1 protein was used to pull down CWN-2, we noticed that more CWN-2 protein was precipitated by CAM-1 (Fig. 4*A* and Fig. S4*C*), suggesting that CAM-1 may possess a higher binding affinity than SAX-3 for CWN-2 molecules. In the presence of both CAM-1 and SAX-3,

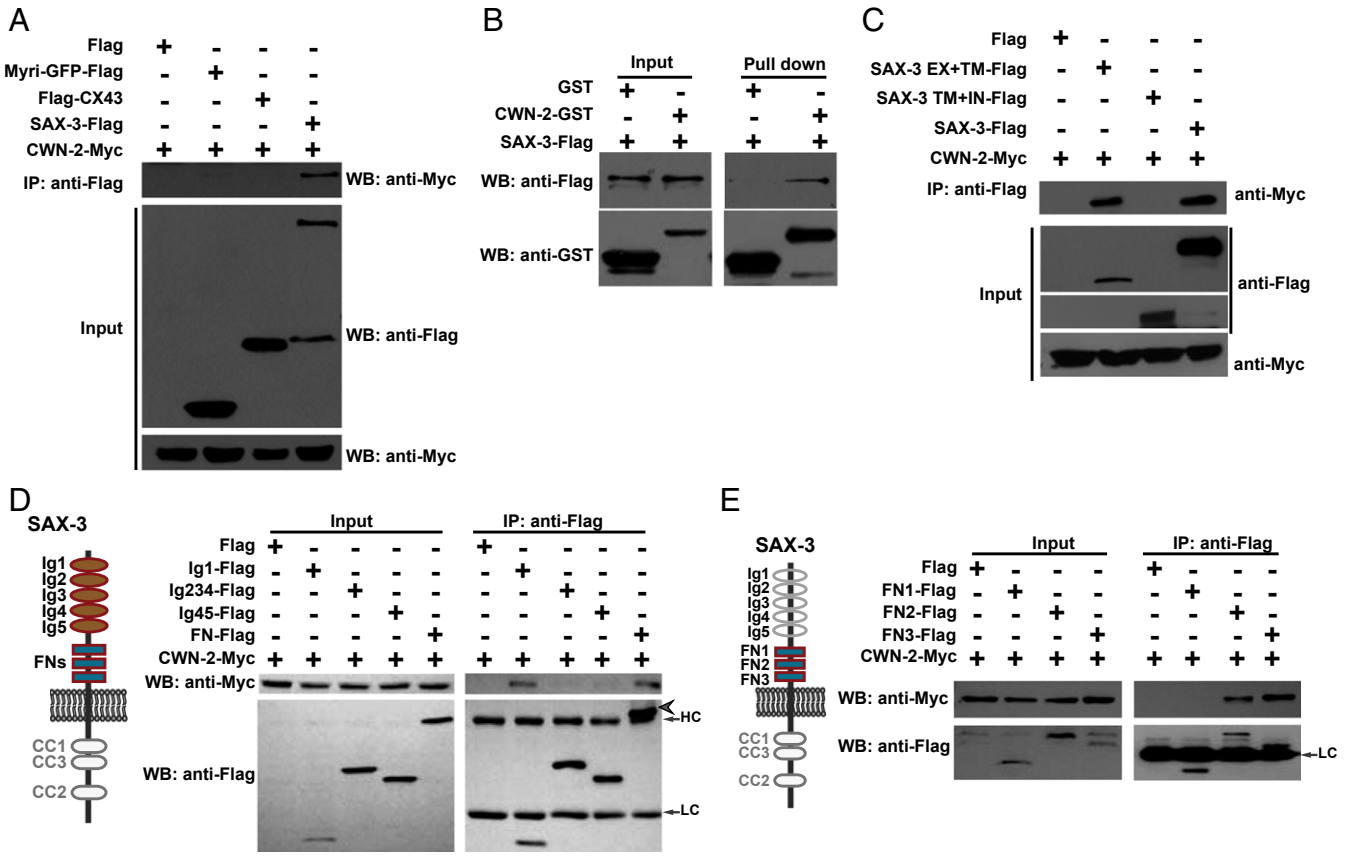

Fig. 3. SAX-3 binds to CWN-2. (*A*) Flag-tagged SAX-3 is associated with Myc-tagged functional CWN-2 in a co-IP assay. (*B*) Purified CWN-2–GST binds to SAX-3–Flag. (*C*) The extracellular domain of SAX-3 (SAX-3 EX) but not the intracellular domain (SAX-3 IN) interacts with CWN-2–Myc. (*D*) Protein–protein interactions between fragments of the SAX-3 extracellular domain and CWN-2–Myc. HC: antibody heavy chain; LC: antibody light chain. The arrowhead indicates the FN-Flag. (*E*) The fibronectin domains 2 and 3 (FN2-Flag and FN3-Flag) bind to CWN-2–Myc.

we found that the amount of precipitated CWN-2 protein was comparable to that observed with CAM-1 alone (Fig. 4*A*).

To test whether Wnt/CWN-2 molecules can be recruited by Robo/SAX-3 or Ror/CAM-1 receptors that are expressed on cell membranes, we first created a CWN-2::GFP–expressing construct. When introduced into worms, this CWN-2::GFP construct rescued the RMED/V neurite outgrowth defect in *cwn-2* mutants (Fig. S4 *A* and *B*), suggesting that the CWN-2::GFP protein is probably functional. When CWN-2::GFP protein was incubated with *Drosophila* S2 cells expressing freely diffusing mCherry, no GFP signal could be detected on the cell surface (Fig. 4*B*). In contrast, when either SAX-3::mCherry or CAM-1::mCherry was expressed in S2 cells, the CWN-2::GFP signal accumulated on the surface of the cells (Fig. 4 *B* and *C*), suggesting that CWN-2 molecules could indeed be recruited to the cell surface by Robo/SAX-3 or Ror/CAM-1 receptor. When we transfected the S2 cells with an equal amount of *sax-3::mCherry* and *cam-1::mCherry* constructs, the cell surface CWN-2::GFP signal was increased compared with *cam-1::mCherry* transfection alone (Fig. 4 *B* and *C*). Because SAX-3 binds to CAM-1, it is a reasonable assumption that by forming a receptor complex with CAM-1, SAX-3 may stabilize the association of CWN-2 with the cell membrane to facilitate CWN-2–mediated signal transduction.

The Role of the Extracellular Domain of SAX-3 in Neurite Outgrowth. Next, we examined whether the association of CWN-2 with the extracellular domain of SAX-3 plays a role in neurite outgrowth in vivo. First, given the ability of SAX-3 to bind to CWN-2, we suspected that the extracellular domain of SAX-3, when overexpressed, may be able to sequester CWN-2 ligands away from CAM-1 and would therefore have a dominant-negative effect on CWN-2 signal transduction. In agreement with this prediction, when we expressed a SAX-3 protein composed only of the extracellular domain on RME cells, we found that the RMED/V neurites were shortened (Fig. S4*D*).

Second, the Ig1 and fibronectin domains of SAX-3 possess the CWN-2-binding activity, so we asked whether these domains are important for SAX-3–mediated neurite outgrowth. We created a series of constructs expressing various truncated SAX-3 proteins. In both *sax-3(ky123)* and *sax-3(ky203)* animals, we found that SAX-3 lacking either the Ig1 or fibronectin domain displayed rescue activity similar to full-length SAX-3 (Fig. 4 *D* and *E* and Fig. S4 *E* and *F*). In contrast, simultaneous deletion of both the Ig1 and fibronectin domains obviously decreased the rescue activity of SAX-3 (Fig. 4 *D* and *E* and Fig. S4 *E* and *F*). We noticed that a significant proportion of rescue activity remained even when both the Ig1 and fibronectin domains were removed (Fig. 4 *D* and *E* and Fig. S4 *E* and *F*), suggesting that the residual intracellular domain of SAX-3 also plays an important role in neurite outgrowth. To confirm the nonessential role of the Ig2, -3, and -4 domains, we used the CRISPR-Cas9 system to create the *sax-3(xd392)* allele, which has an in-frame deletion of the Ig2, Ig3, and Ig4 domains, while leaving the Ig1 and fibronectin domains intact. Compared with other *sax-3* alleles, for example *xd394*, which contains a frame-shift mutation after Ig1, the *sax-3(xd392)* allele displays almost no outgrowth defects (Fig. S4 *G* and *H*). Taken together, these results provide evidence that the

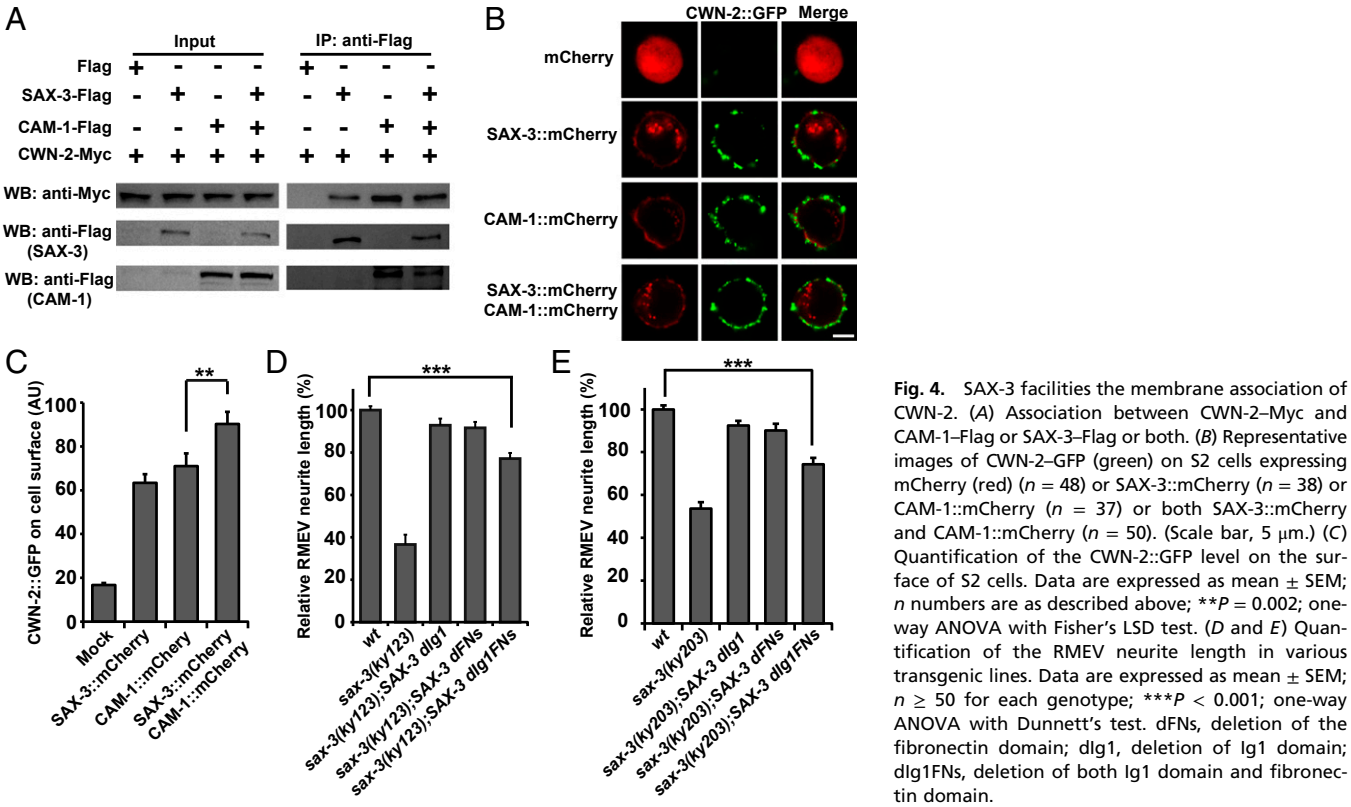

Fig. 4. SAX-3 facilities the membrane association of CWN-2. (*A*) Association between CWN-2–Myc and CAM-1–Flag or SAX-3–Flag or both. (*B*) Representative images of CWN-2–GFP (green) on S2 cells expressing mCherry (red) ($n = 48$) or SAX-3::mCherry ($n = 38$) or CAM-1::mCherry ($n = 37$) or both SAX-3::mCherry and CAM-1::mCherry ($n = 50$). (Scale bar, 5 μm.) (*C*) Quantification of the CWN-2::GFP level on the surface of S2 cells. Data are expressed as mean ± SEM; *n* numbers are as described above; $^{**}P = 0.002$; one-way ANOVA with Fisher's LSD test. (*D* and *E*) Quantification of the RMEV neurite length in various transgenic lines. Data are expressed as mean ± SEM; $n \geq 50$ for each genotype; $^{***}P < 0.001$; one-way ANOVA with Dunnett's test. dFNs, deletion of the fibronectin domain; dIg1, deletion of Ig1 domain; dIg1FNs, deletion of both Ig1 domain and fibronectin domain.

extracellular domain of SAX-3 receptor can sense CWN-2 during RMED/V neurite outgrowth.

SAX-3 Binds to DSH-1. Our previous study showed that the CAM-1 ICD binds to DSH-1 in yeast two-hybrid assays (17). Additional co-IP assays confirmed that CAM-1 ICD indeed binds to DSH-1 (Fig. S5*A*). Interestingly, when we incubated CAM-1 ICD and DSH-1 together with SAX-3 ICD, we found that the amount of DSH-1 protein associated with CAM-1 ICD was significantly increased (Fig. 5 *A* and *B*). It has been proposed that the recruitment of Dsh protein to membrane receptors may trigger Dsh phosphorylation in mammals (20, 31). When DSH-1 was incubated with CAM-1 ICD and SAX-3 ICD, two DSH-1 protein bands with different sizes were observed (Fig. S5*B*). Treatment with calf intestinal alkaline phosphatase (CIAP) significantly decreased the level of the larger DSH-1 band (Fig. S5*B*). In addition, when we probed the DSH-1 protein with an antibody against phosphorylated Tyrosine (anti-pTyr), the anti-pTyr^{+} band disappeared after CIAP treatment (Fig. S5*B*). Interestingly, when SAX-3 ICD was present, the level of phosphorylated DSH-1 associated with CAM-1 was significantly increased, implying that the DSH-1 signal can be enhanced by the SAX-3 receptor (Fig. S5 *C* and *D*).

How does SAX-3 help DSH-1 to associate with CAM-1? We expressed SAX-3 ICD and DSH-1 in HEK293T cells and found that SAX-3 ICD is associated with DSH-1 (Fig. 5*C*). The SAX-3 intracellular region contains three conserved cytosolic (CC) domains, which are CC1, CC3, and CC2 in sequence (4) (Fig. 5*D*). To identify the specific region involved in DSH-1 binding, we further performed structure-function analysis using various truncated forms of the SAX-3 protein. As shown in Fig. 5*D*, the membrane proximity region and the CC domains associated with DSH-1. Among the three CC domains, the CC2 domain appears to contain the strongest DSH-1 binding activity. Thus, SAX-3 may convey DSH-1 to CAM-1 through its association with DSH-1 via multiple binding sites.

SAX-3 Forms a Complex with CAM-1 and DSH-1. In addition to DSH-1, SAX-3 ICD also associates with CAM-1. Additional co-IP experiments with a series of truncated SAX-3 fragments suggested that both the membrane proximity region and the N-terminal portion containing the CC2 domain were able to bind to CAM-1 ICD (Fig. S5*E*). Conversely, in CAM-1, the kinase domain and the region close to the transmembrane motif were able to bind to SAX-3 (Fig. S5*F*).

Based on the above data, we wondered whether SAX-3, CAM-1, and DSH-1 function in the same complex. To test this theory, we performed a two-step co-IP. We first pulled down Flag-tagged CAM-1 ICD using anti-Flag antibody, then detected the presence of DSH-1 and SAX-3 ICD. Next, we immunoprecipitated the Flag-tagged sample with anti-His antibody to pull down the Myc-His double-tagged SAX-3 ICD fragment and analyzed the pull-down sample with anti-Myc and anti-Flag antibodies. As shown in Fig. 5*E*, both CAM-1 ICD and DSH-1 were present in the SAX-3 ICD-containing sample, suggesting that the CAM-1, SAX-3, and DSH-1 proteins form a complex. Consistent with this notion, we found that *sax-3*/+;*cam-1*/+;*dsh-1*/+ triple heterozygote animals displayed evidently shortened neurites (Fig. 5*F*). In contrast, neither *cam-1*/+;*dsh-1*/+ double heterozygotes nor any of the *sax-3*/+, *cam-1*/+, *dsh-1*/+ single heterozygotes showed any distinctive neurite outgrowth defect (Fig. 5*F* and Fig. S5*G*). Furthermore, although SAX-3 without the membrane proximity region, the CC1–CC3 domains, or the CC2 domain possessed some rescue activity, SAX-3 lacking the intracellular domain almost completely lost its rescue capability (Fig. 5*G* and Fig. S5*H*), implying that the intracellular scaffolding activity is critical for SAX-3 function.

SAX-3 Regulates the Asymmetric Distribution of DSH-1. We further tested the function of SAX-3 in a cellular context in vivo. First, we examined the subcellular localization of the SAX-3 protein in developing RMED/V neurons. To do that, we created a functional

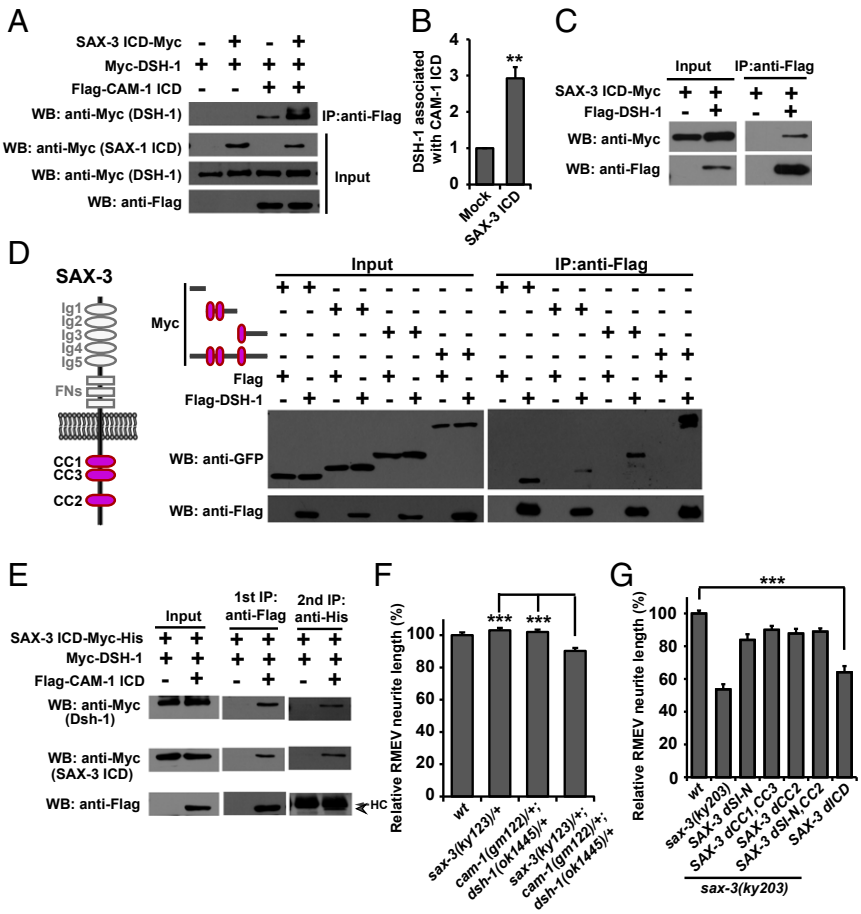

Fig. 5. SAX-3 forms a complex with CAM-1 and DSH-1. (*A*) In the presence of Myc-tagged SAX-3 ICD, the amount of DSH-1 protein associated with CAM-1 ICD is increased. (*B*) Quantification of the DSH-1 level associated with CAM-1 ICD. Data are expressed as mean ± SEM; $n = 5$; $^{**}P = 0.005$; two-tailed paired Student's *t* test. (*C*) Myc-tagged SAX-3 ICD associates with Flag–DSH-1. (*D*) Protein–protein interactions between truncated SAX-3 ICD and Flag–DSH-1. (*E*) Sequential co-IP tests. The arrowhead points to the Flag–CAM-1 ICD band. HC, antibody heavy chain. (*F*) Quantification of the RMEV neurite length. Data are expressed as mean ± SEM; $n \geq 50$ for each genotype; $^{***}P < 0.001$; one-way ANOVA with Bonferroni's test. (*G*) Quantification of the RMEV neurite length in various rescuing lines. Data are expressed as mean ± SEM; $n \geq 50$ for each genotype; $^{***}P < 0.001$; one-way ANOVA with Dunnett's test. dCC1, CC3, deletion of both CC1 and CC3; dCC2, deletion of CC2; dICD, deletion of the entire intracellular domain; dSI-N, deletion of the membrane proximity region; dSI-N,CC2, deletion of both the membrane proximity region and the CC2 region.

SAX-3::GFP construct driven by its endogenous promoter, which when introduced into *sax-3(ky203)* worms efficiently rescued the shortened neurite phenotype in *sax-3(ky203)* (Fig. 2 *B* and *C*). *sax-3* expression begins around the midembryonic stage (350 min) and is restricted to the anterior region of an embryo (Fig. S6*A*, *Upper*), where the neurons or neuroblast cells are clustered. As shown in Fig. S6*A*, SAX-3::GFP is distributed on the membrane surfaces of those cells. When embryos progressed to the late-embryonic stage (500 min), we detected SAX-3::GFP on RME cells (Fig. S6*A*, *Lower*, arrow). However, *sax-3* is widely expressed in many neurons and the distinctive subcellular localization of SAX-3 on RMED/V neurons, if there is any, could easily be masked by the SAX-3::GFP signal from surrounding cells. Therefore, we generated SAX-3::GFP driven by the *unc-25* promoter. By coexpressing P*unc-25*::mCherry in *unc-30* to specifically visualize RME cells, we were able to detect the subcellular localization of SAX-3 protein on RME neurons. The posterior RMED/V neurites continuously extend during larval stages (17) and we found that SAX-3::GFP is distributed on the elongating neurites (Fig. 6 *A* and *B*, arrows). The SAX-3::GFP expression sometimes induces ectopic neurite growth and the SAX-3::GFP signal is localized on those ectopic neurites as well (Fig. 6*B*, arrowheads). Intriguingly, SAX-3::GFP is asymmetrically distributed on the posterior sides of RMED and RMEV cell bodies, from which the neurites are elongating (Fig. 6 *A* and *B*).

Coincidentally, the functional DSH-1::GFP is also asymmetrically distributed on the growing neurites and the posterior side of RMED/V cell bodies (Fig. 6 *C* and *E*). When we removed *sax-3* by *sax-3(ky203)* mutation, we found that the asymmetric distribution of the DSH-1::GFP on RMED/V neurons is disrupted (Fig. 6 *D* and *E*). In addition, the expression level of DSH-1::GFP on the extending neurites is somewhat decreased (Fig. S6 *C*–*E*). Taken together, these results provide evidence that *sax-3* may promote directional neurite outgrowth by enhancing the asymmetric distribution of DSH-1 protein in vivo.

CWN-2 and CAM-1 Do Not Exert Their Regulatory Effect on Neurite Outgrowth by Patterning the Asymmetric Localization of DSH-1. We noticed that the overexpression of *dsh-1* in RME cells induces ectopic neurites from both RMED and RMEV neurons (Fig. S6*B*, arrowheads), implying a correlation between *dsh-1* expression level and neurite outgrowth capacity. When *cam-1* or *cwn-2* was removed, neurites were unable to extend, regardless of whether they were ectopic ones or regular posterior neurites from RMED/V cells. This suggests that the outgrowth activity executed by DSH-1 protein is dependent on upstream CWN-2 cues and the signaling receptor CAM-1. In *cwn-2(ok895)*–null animals, the asymmetric distribution of DSH-1 on RMED/V cells is not altered (Fig. 6*F* and Fig. S6*F*). In *cam-1(ks52)* animals, the intracellular domain of CAM-1 is largely removed, and the asymmetric distribution of DSH-1 is also unaffected (Fig. 6*G* and Fig. S6*F*). Furthermore, when we examined the SAX-3 localization in *cwn-2(ok895)* mutants, we found that the posteriorly enriched SAX-3::GFP pattern is indistinguishable from wild-type (Fig. S6*G*). Given the fact that RMED/V neurite outgrowth is greatly affected by the CWN-2 ligand and CAM-1 receptor, we would like to propose that the Wnt/CWN-2 ligand and Ror/CAM-1 receptor probably regulate neurite outgrowth by activating DSH-1. Meanwhile, Robo/SAX-3 receptor functions as a coreceptor with Ror/CAM-1 for Wnt/CWN-2 and patterns the specific subcellular localization of DSH-1 protein to facilitate directional neurite outgrowth in vivo.

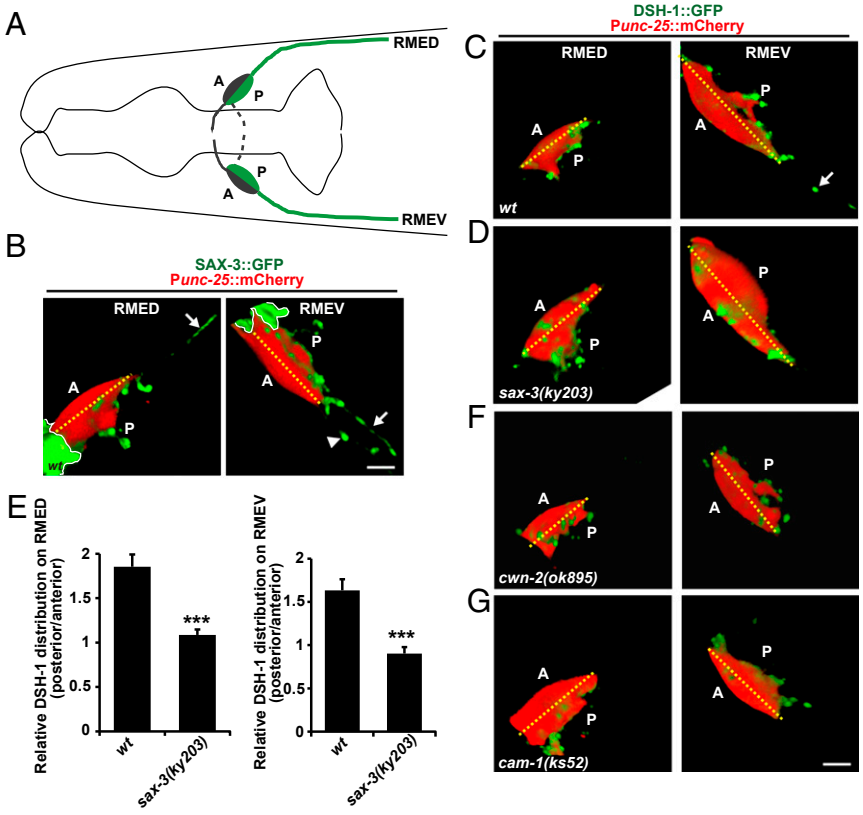

Fig. 6. The asymmetric localization of DSH-1 requires SAX-3. (*A*) Schematic drawing of the RMED and RMEV neurons. A, anterior; P, posterior. (*B*) SAX-3::GFP (green) distribution on RMED and RMEV neuron cell bodies (red) in 3D reconstructions. The dashed yellow line divides the cell body into anterior and posterior domains. The yellow lines indicate the nerve ring region. White arrows indicate the posterior neurites of RMED/V neurons. The arrowhead indicates an ectopic neurite. (Scale bar, 2 μm.) (*C* and *D*) DSH-1::GFP (green) distribution on RMED and RMEV neuron cell bodies (red) in 3D reconstructions in wild-type (*C*) and *sax-3(ky203)* mutants (*D*). (*E*) Quantification of the enrichment of DSH-1::GFP in wild-type and *sax-3(ky203)* mutants. Data are expressed as mean ± SEM. For RMED, *wt* $n = 13$ and *sax-3(ky203)* $n = 13$; for RMEV, *wt* $n = 7$ and *sax-3(ky203)* $n = 14$; ***$P < 0.001$; two-tailed unpaired Student's *t* test. (*F* and *G*) DSH-1::GFP (green) distribution in *cwn-2(ok895)* and *cam-1(ks52)* mutant RMED/V cells. (Scale bar, 2 μm.)

Discussion

Genetics and biochemistry have identified the key molecules involved in axon guidance and provided important insights into what these molecules do. Here, we have identified a new mechanistic link between Robo receptor and the Wnt-Ror-Dsh pathway, which is certain to advance our understanding of how these molecules interact in space and time to orchestrate the dynamic process of growth cone navigation through a complex biological environment.

In agreement with our findings, evidence from multiple model systems has revealed that Robo receptors have Slit-independent functions. For example, Slits are not the only midline repellents in the mouse central nerve system, and many axons still cross normally in Slit triple-knockout embryos (32, 33). More recently, it was shown that mammalian Robo3 receptor does not bind to Slits. Robo3 also interacts with the netrin–DCC chemoattractive signaling pathway (10). In addition, NELL2, which is expressed by motoneurons in the mouse ventral spinal cord, acts as a repulsive ligand for Robo3 (7). Furthermore, while the Robo/SAX-3 receptor has a profound effect on nerve ring organization in *C. elegans*, the sole Slit plays a rather minor role in this process (14). *sax-3* mutants have midline crossing defects in the ventral nerve cord; however, corresponding defects are not found in *slit-1* mutants (34).

Previous studies hinted that Robo may function in Wnt-mediated processes. For example, Slit2-Robo1 cooperates with R-spondin1 to activate Wnt signaling and promote intestinal repair (35). Robo/SAX-3 is involved in the anterior–posterior cell migration of the *C. elegans* CAN neuron (34), which is strongly influenced by Wnt ligands and Ror receptor (16, 36). Both Slit/Slt-1 and Wnt/CWN-2 are expressed in the anterior region of the worm (17, 34), but only CWN-2 has a strong impact on the organization of the nerve ring bundle (14). Interestingly, both Robo/SAX-3 and Ror/CAM-1 function in SIA and SIB neurons to facilitate nerve ring placement (14), implying that Robo functions in the same cell as the Ror receptor. Here, we provide direct evidence that Robo/SAX-3 receptor binds to Wnt/CWN-2 ligand and may function in a receptor complex with Ror/CAM-1 receptor. Our findings offer a plausible explanation for how a Robo receptor participates in Wnt-mediated biological processes. The enhanced but not additive effect between CAM-1 and SAX-3 on the membrane association of CWN-2 hints that CAM-1 and Robo likely function in a common receptor complex and probably bind to the same CWN-2 molecule. The presence of SAX-3 receptor may therefore improve CWN-2 recognition, thus facilitating CWN-2 signal transduction. Taking all of the genetic and biochemical analyses together, a conceivable model is that Ror/CAM-1 acts as a major receptor to sense and respond to CWN-2 signal, while the SAX-3 receptor plays a more regulatory role in this process, possibly stabilizing the association of CWN-2 with membrane receptors.

The role of Frz receptor in RMED/V neurite outgrowth is intriguing and inspires us to think about how Wnt signaling can be regulated in a complex manner at the receptor level. The *C. elegans* genome encodes four Frz receptors. Among them, MIG-1 and CFZ-2 play redundant roles in Wnt signaling. Single mutations in either *mig-1* or *cfz-2* result in mild or variable neurite outgrowth defects (17). When both MIG-1 and CFZ-2 are removed, the neurite outgrowth defect is more severe, mimicking that observed in *cam-1*, *cwn-2*, or *dsh-1* nulls (17). These data suggest that Frz receptors are also vital for Wnt signaling, but in a redundant manner. Interestingly, when both the SAX-3 receptor and CFZ-2 are absent, Wnt signaling is also reduced to a minimal level and the RMED/V neurites do not grow. Thus, SAX-3 can also function with Frz receptors to regulate Wnt signaling. The complex genetic interactions revealed by this and previous studies (17) suggest that different receptors, including Frz, Ror, and Robo, may form multiple receptor complexes by combining in various ways to respond to Wnt cues. In double mutants between a null allele of *sax-3* and an allele of *cam-1*, in which the intracellular domain is disrupted, the phenotype

resembles the scenario in which CWN-2 signaling is completely blocked. Therefore, it is reasonable to propose that Robo receptor can assist both Ror and Frz receptors to transmit Wnt signals.

Robo receptors are single-pass transmembrane proteins with no autocatalytic or enzymatic activity in their intracellular region, suggesting that they depend on downstream signaling and scaffolding molecules to mediate their functions. Indeed, Robo receptors have been implicated in associations with Frazzled/DCC/UNC-40 (3), Ephrin receptor (37), EVA-1 (38), and others (39, 40). What then is the biological significance of the Robo–Ror receptor complex in Wnt signaling? The directional outgrowth of RMED/V neurites require Rho/MIG-2 and Rac/CED-10, suggesting that the planar cell polarity (PCP) pathway may be activated (17). It is notable that recent work in vertebrates suggests that the Ror2 receptor, which serves as a Wnt5 coreceptor with Frizzled, is a newly identified core component of PCP (41). Wnt5 induces Dsh phosphorylation through Ror1 and Ror2 (20). Although the function of Dsh phosphorylation in PCP remains unclear, the phosphorylation of Dsh is often used as a readout for Wnt activation (42) and multiple kinases have been found to associate with Dsh and phosphorylate it (43). The observations that the presence of Robo increases the amount of Dsh protein associated with Ror but does not alter the phosphorylation level of Dsh suggest that Robo can facilitate the recruitment of activated Dsh protein. The PCP pathway is critical for the generation of both global and local directional information, which is the key to breaking symmetry and creating the complex organizational pattern of living organisms. In particular, the asymmetric subcellular localization of Dsh is tightly linked to the polarized action of a cell. For example, during the development of the *Drosophila* wing, Dsh protein specifically accumulates at the distal edges, but not at the proximal edges (44). In our study, the asymmetric distribution of Dsh fits well with the polarized neurite growth, and supports the notion that polarized Dsh distribution is crucial for polarized cell behavior. Like Dsh, Robo is also unevenly distributed. Without Robo, the asymmetric distribution of Dsh is disrupted, and the directional growth of RMED/V neurites is impaired. The Wnt ligand and Ror receptor regulate Dsh-mediated neurite outgrowth, but do not control the polarized distribution of Dsh protein. Therefore, we propose that Robo, as part of a membrane receptor complex with Ror, facilitates the establishment of a polarized signaling apparatus centered on Dsh, and thus converts the unevenly distributed Wnt signal to a polarized intracellular response. Intriguingly, the polarized subcellular localization of Robo/SAX-3 is not dependent on Wnt/CWN-2. Hence, the molecular identity of the signals that pattern the distribution of the Robo receptor remains to be determined. In *C. elegans*, the other four Wnts are able to bypass the loss of CWN-2 in mediating neurite outgrowth, suggesting that the functional requirement for CWN-2 in neurite outgrowth is not due to its intrinsic molecular features (17). Considering the pleiotropic functions of Wnts and the mechanistic conservation underling Wnt signaling in many biological processes, the role of Robo receptor in facilitating Wnt signaling is likely to extend to different Wnts in a wide range of species.

Methods

Worm Strains and Genetics. Strain maintenance and genetic manipulation were performed as described previously (45). *juIs76* is a transgenic line of *Punc-25::GFP* labeling GABA motor neurons. Mutants and transgenic fluorescence reporters used in this study are: LG I: *eva-1(ok1133)*, *mig-1(e1787)*; LGII: *cam-1(ks52)*, *cam-1(gm105)*, *cam-1(gm122)*, *dsh-1(ok1445)*, *juIs76*, *xdIs121(Punc-25::mCherry)*; LGIV: *unc-30(ju54)*, *srgp-1(ok300)*, *cwn-2(xd1)*, *cwn-2(ok895)*; LGV: *cfz-2(ok1201)*; LGX: *sax-3(ky123)*, *sax-3(ky200)*, *sax-3(ky203)*, *sax-3(xd392)*, *sax-3(xd394)*, *slt-1(eh15)*. Additional transgenic lines are: *xdEx1219(Psax-3::GFP,rol-6)*, *xdEx1336(Psax-3::sax-3::GFP,Podr-1::RFP)*, *xdEx1436(Pcam-1b::sax-3,Podr-1::RFP)*, *xdEx1449(Psnb-1::sax-3,Podr-1::RFP)*, *xdEx1436(Punc-47::sax-3,Podr-1::RFP)*, *xdEx1469(Punc-25::sax-3,Podr-1::RFP)*, *xdEx1470(Punc-86::sax-3,Podr-1::RFP)*, *xdEx1472(Phlh-17::sax-3,Podr-1::RFP)*, *xdEx1865(Punc-25::dsh-1::gfp;Punc-122-RFP)*, *xdEx2027(Psax-3::sax-3::gfp;Punc-122::RFP)*, *xdEx2024(Punc-25::sax-3::gfp;Punc-122::RFP)*, *xdEx2058(Pcwn-2::cwn-2::gfp;Podr-1::RFP)*, *xdEx2059(Pcwn-2::cwn-2::3Myc;Punc-122::RFP)*, *xdEx1991(Psax-3::sax-3-dSI-N;Punc-122::RFP)*, *xdEx1992(Psax-3::sax-3-dCC1,CC3;Punc-122::RFP)*, *xdEx1993(Psax-3::sax-3-dCC2;Punc-122::RFP)*, *xdEx1994(Psax-3::sax-3-dSI-N,CC2;Punc-122::RFP)*, *xdEx2022(Psax-3::sax-3-dICD;Punc-122::RFP)*, *xdEx2050(Psax-3::sax-3-dlg1;Podr-1::RFP)*, *xdEx2060(Psax-3::sax-3-dFNs;Podr-1::RFP)*, and *xdEx2067(Psax-3::sax-3-dlg1FNs;Podr-1::RFP)*, *xdEx2093(psax-3-NLSGFPL;punc-122-RFP)*, *xdEx2094(punc-25-cas9-sgS5-S6;odr-1-RFP line1)*, *xdEx2095(punc-25-cas9-sgS5-S6;odr-1-RFP line2)*.

DNA Constructs and Transgenic Animals. The complete *sax-3* cDNA was amplified from *sax-3* cDNAs kindly provided by Cornelia I. Bargmann, The Rockefeller University, New York, and Yuji Kohara, National Institute of Genetics, Japan. The full-length and different truncated forms of *sax-3* cDNAs were cloned into pPD95.75 and dpSM vectors. The promoter region of *sax-3* comprised 4.0 kb of upstream genomic DNA. Other promoters (*pcam-1b*, *psnb-1*, *punc-47*, *punc-25*, *punc-86*, *phlh-17*) used for rescue were cloned into dpSM-*sax-3*. Transgenic animals were produced as previously described (18). Integrated strains were obtained by UV irradiation. All integrated transgenic animals were out-crossed at least three times.

Image Collection and Quantification. Images of mutants and S2 immunostaining were captured using a Leica SP8 confocal microscope. The images of SAX-3 expression were captured using an Olympus confocal microscope. All images were taken at the young adult stage unless specifically indicated. Images of RMED and RMEV were analyzed with ImageJ software. The lengths of RME neurites and the worm body were measured. The relative length of RME was normalized with body length. The relative length of RME in mutants was normalized with wild-type. Images of S2 immunostaining were also analyzed with ImageJ software. The area of S2 cells and mean signal intensity were measured and the signal intensity was then normalized with the perimeter. All error bars represent SEM. Statistical analyses were performed with Student's *t* test. For each genotype, more than 50 animals were imaged. More than 30 S2 cells were imaged and analyzed for each group. Images of the subcellular localization of SAX-3-GFP or DSH-1::GFP on the cell surface of RME neuron cell bodies were captured and reconstructed in 3D forms by a Leica SP8 confocal microscope. The ratio of the GFP signal intensity on the posterior side of RMED/V cell body over the signal on the anterior side is defined as the relative SAX-3 or DSH-1 distribution on RMED or RMEV. For DSH-1::GFP protein on RMED/V neurites, the mean DSH-1::GFP level was measured and then normalized with the DSH-1::GFP level on RMED or RMEV cell bodies.

Cell Culture and Transfection. The HEK293T cell line was used for protein expression. The cells were maintained in DMEM containing 12% FBS. For cell transfection, Polyethylenimine (Polysciences) was used according to the manufacturer's instructions. The clones used for transfection were constructed in pcDNA3.1/myc-His (–) and pFLAG-CMV-2 or their modified forms. C-terminal tags, such as GST, GFP, Flag-His, and so on, were cloned into pcDNA3.1/myc-His (–) by replacing the myc-His tag. Cultured cells were harvested 24 h after transfection. The *Drosophila* S2 cells were cultured in Sf-900 II serum-free medium (Gibco) at 28 °C. For protein expression in S2 cells, the pUAST expression vector was used. mCherry and other tags were cloned into the C terminus between the Kpn1 and Xba1 sites. The expression plasmids were transfected together with actin-GAL4 by Cellfectin II (Invitrogen) and PLUS reagent (Invitrogen). S2 cells were harvested 48 h after transfection.

Immunoprecipitation and Western Blot. The cell cultures were lysed using 1% Nonidet P-40 lysis buffer (50 mM Tris·HCl, 150 mM NaCl, 1% Nonidet P-40, pH 7.6) containing protease mixture inhibitor (Roche). After lysis for 30 min on ice and centrifugation at 13,400 × *g* for 15 min at 4 °C, the protein supernatant was incubated with anti-FLAG M2 affinity gel (Sigma) for 4 h at 4 °C. The immunoprecipitates were washed three times with lysis buffer and boiled for 10 min in SDS sample buffer containing DTT. Agarose-conjugated anti–His-Tag (MBL) was used for His-Tag protein immunoprecipitation. For GFP-tagged protein immunoprecipitation, anti-GFP antibody ab290 (Abcam) was used at 1:10,000 dilution and incubated with the protein supernatant overnight at 4 °C, then protein A Sepharose (GE Healthcare Life Sciences) was added and incubated for 4 h to precipitate the GFP-tagged proteins. For purified proteins, the immunoprecipitates were eluted with elution buffer (Thermal Scientific) and neutralized with Tris buffer (pH 9.0). For Western blotting, the samples were separated on SDS/PAGE denaturing gels and transferred to nitrocellulose membranes (Pall Life Sciences). Membranes were blocked with 5% dry milk and signals were visualized with Supersignal West Pico Substrate kit (Pierce). The following antibodies were used in Western blotting: anti-FLAG M2 (1:5,000; Sigma), MYC-Tag (19C2) mouse

mAb (1:5,000; Abmart), antiphosphotyrosine (4G10) mAb (1:1,000; Millipore), anti- GFP pAb (1:5,000; MBL), anti–HA-tag mAb (1:5,000; MBL), and anti–Myc-tag pAb (1:5,000; MBL). For the CAM-1–Flag or SAX-3–Flag and CWN-2–Myc binding assays, the coimmunoprecipitated CWN-2–Myc protein was normalized with the input level.

GST Pull-Down Assay. GST and GST–CWN-2 were expressed in HEK293T cells, and the cells were lysed using 1% Nonidet P-40 lysis buffer (50 mM Tris·HCl, 150 mM NaCl, 1% Nonidet P-40, pH 7.6) containing protease mixture inhibitor (Roche) for 30 min on ice and centrifuged at 13,400 × *g* for 15 min at 4 °C. The supernatants were incubated with Glutathione Sepharose 4B (GE Healthcare) at 4 °C for 4 h. After washing with PBS three times, the Sepharose was incubated with purified Flag–SAX-3 at 4 °C overnight. The Sepharose was washed three times with PBS and boiled in SDS sample buffer.

S2 Immunostaining. S2 cells expressing SAX-3–mCherry, CAM-1–mCherry, or mCherry alone were harvested 48 h after transfection and incubated for 4 h in Sf-900 II serum-free medium (Gibco) containing CWN-2–GFP. The treated cells were then cultured on coverslips coated with poly-lysine (Sigma) for another 4 h. The medium was removed and the cells were washed with TBS buffer three times. Next, 4% PFA was used for fixation for 1 h. After washing with TBS three times, the S2 cells were incubated with anti-GFP antibody (ab290; Abcam) overnight at 4 °C. Alexa Fluor 488 donkey anti-rabbit IgG (H+L) (Life Technologies) was used for immunostaining.

Statistical Analysis. All graphical data are presented as mean ± SEM. Two-tailed unpaired and paired Student's *t* tests were performed for comparison between two groups of samples. To compare multiple groups, one-way ANOVA was used with an appropriate multiple comparisons post hoc test (the test used is stated in each figure legend). $*P < 0.05$; $**P < 0.01$; $***P < 0.001$; NS, not significant.

ACKNOWLEDGMENTS. We thank Drs. Bo Zhang, Song Song, and Hui Sun for initiating the work; and Drs. Yishi Jin, Cori Bargmann, Xun Huang, Mei Zhen, and Kang Shen, the *Caenorhabditis elegans* Gene Knockout Consortium, and the *Caenorhabditis* Genetics Center for providing reagents, strains, and technical support. This work was supported by the National Natural Science Foundation of China (Grant 31490593) and the National Basic Research Program of China (Grants 2016YFA0501000 and 2014CB942803).

1. Hedgecock EM, Culotti JG, Hall DH (1990) The unc-5, unc-6, and unc-40 genes guide circumferential migrations of pioneer axons and mesodermal cells on the epidermis in *C. elegans*. *Neuron* 4:61–85.
2. Colamarino SA, Tessier-Lavigne M (1995) The axonal chemoattractant netrin-1 is also a chemorepellent for trochlear motor axons. *Cell* 81:621–629.
3. Stein E, Tessier-Lavigne M (2001) Hierarchical organization of guidance receptors: Silencing of netrin attraction by slit through a Robo/DCC receptor complex. *Science* 291:1928–1938.
4. Kidd T, et al. (1998) Roundabout controls axon crossing of the CNS midline and defines a novel subfamily of evolutionarily conserved guidance receptors. *Cell* 92: 205–215.
5. Kidd T, Bland KS, Goodman CS (1999) Slit is the midline repellent for the robo receptor in *Drosophila*. *Cell* 96:785–794.
6. Brose K, et al. (1999) Slit proteins bind Robo receptors and have an evolutionarily conserved role in repulsive axon guidance. *Cell* 96:795–806.
7. Jaworski A, et al. (2015) Operational redundancy in axon guidance through the multifunctional receptor Robo3 and its ligand NELL2. *Science* 350:961–965.
8. Camurri L, et al. (2005) Evidence for the existence of two Robo3 isoforms with divergent biochemical properties. *Mol Cell Neurosci* 30:485–493.
9. Mambetisaeva ET, Andrews W, Camurri L, Annan A, Sundaresan V (2005) Robo family of proteins exhibit differential expression in mouse spinal cord and Robo-Slit interaction is required for midline crossing in vertebrate spinal cord. *Dev Dyn* 233: 41–51.
10. Zelina P, et al. (2014) Signaling switch of the axon guidance receptor Robo3 during vertebrate evolution. *Neuron* 84:1258–1272.
11. Sabatier C, et al. (2004) The divergent Robo family protein rig-1/Robo3 is a negative regulator of slit responsiveness required for midline crossing by commissural axons. *Cell* 117:157–169.
12. Zallen JA, Yi BA, Bargmann CI (1998) The conserved immunoglobulin superfamily member SAX-3/Robo directs multiple aspects of axon guidance in *C. elegans*. *Cell* 92: 217–227.
13. Yu TW, Hao JC, Lim W, Tessier-Lavigne M, Bargmann CI (2002) Shared receptors in axon guidance: SAX-3/Robo signals via UNC-34/enabled and a netrin-independent UNC-40/DCC function. *Nat Neurosci* 5:1147–1154.
14. Kennerdell JR, Fetter RD, Bargmann CI (2009) Wnt-Ror signaling to SIA and SIB neurons directs anterior axon guidance and nerve ring placement in *C. elegans*. *Development* 136:3801–3810.
15. Clevers H, Nusse R (2012) Wnt/β-catenin signaling and disease. *Cell* 149:1192–1205.
16. Forrester WC, Dell M, Perens E, Garriga G (1999) A *C. elegans* Ror receptor tyrosine kinase regulates cell motility and asymmetric cell division. *Nature* 400:881–885.
17. Song S, et al. (2010) A Wnt-Frz/Ror-Dsh pathway regulates neurite outgrowth in *Caenorhabditis elegans*. *PLoS Genet* 6:e1001056.
18. Paganoni S, Ferreira A (2005) Neurite extension in central neurons: A novel role for the receptor tyrosine kinases Ror1 and Ror2. *J Cell Sci* 118:433–446.
19. Hayashi Y, et al. (2009) A trophic role for Wnt-Ror kinase signaling during developmental pruning in *Caenorhabditis elegans*. *Nat Neurosci* 12:981–987.
20. Ho HY, et al. (2012) Wnt5a-Ror-Dishevelled signaling constitutes a core developmental pathway that controls tissue morphogenesis. *Proc Natl Acad Sci USA* 109: 4044–4051.
21. Francis MM, et al. (2005) The Ror receptor tyrosine kinase CAM-1 is required for ACR-16-mediated synaptic transmission at the *C. elegans* neuromuscular junction. *Neuron* 46:581–594.
22. Jensen M, et al. (2012) Wnt signaling regulates acetylcholine receptor translocation and synaptic plasticity in the adult nervous system. *Cell* 149:173–187.
23. Sulston JE, Schierenberg E, White JG, Thomson JN (1983) The embryonic cell lineage of the nematode *Caenorhabditis elegans*. *Dev Biol* 100:64–119.
24. White JG, Southgate E, Thomson JN, Brenner S (1986) The structure of the nervous system of the nematode *Caenorhabditis elegans*. *Philos Trans R Soc Lond B Biol Sci* 314:1–340.
25. Forrester WC, Garriga G (1997) Genes necessary for *C. elegans* cell and growth cone migrations. *Development* 124:1831–1843.
26. Shen Z, et al. (2014) Conditional knockouts generated by engineered CRISPR-Cas9 endonuclease reveal the roles of coronin in *C. elegans* neural development. *Dev Cell* 30:625–636.
27. Fan X, Labrador JP, Hing H, Bashaw GJ (2003) Slit stimulation recruits Dock and Pak to the roundabout receptor and increases Rac activity to regulate axon repulsion at the CNS midline. *Neuron* 40:113–127.
28. Zaidel-Bar R, et al. (2010) The F-BAR domain of SRGP-1 facilitates cell-cell adhesion during *C. elegans* morphogenesis. *J Cell Biol* 191:761–769.
29. Wong K, et al. (2001) Signal transduction in neuronal migration: Roles of GTPase activating proteins and the small GTPase Cdc42 in the Slit-Robo pathway. *Cell* 107: 209–221.
30. Green JL, Inoue T, Sternberg PW (2007) The *C. elegans* ROR receptor tyrosine kinase, CAM-1, non-autonomously inhibits the Wnt pathway. *Development* 134:4053–4062.
31. González-Sancho JM, et al. (2013) Functional consequences of Wnt-induced dishevelled 2 phosphorylation in canonical and noncanonical Wnt signaling. *J Biol Chem* 288: 9428–9437.
32. Long H, et al. (2004) Conserved roles for Slit and Robo proteins in midline commissural axon guidance. *Neuron* 42:213–223.
33. Zou Y, Stoeckli E, Chen H, Tessier-Lavigne M (2000) Squeezing axons out of the gray matter: A role for slit and semaphorin proteins from midline and ventral spinal cord. *Cell* 102:363–375.
34. Hao JC, et al. (2001) *C. elegans* slit acts in midline, dorsal-ventral, and anterior-posterior guidance via the SAX-3/Robo receptor. *Neuron* 32:25–38.
35. Zhou WJ, Geng ZH, Spence JR, Geng JG (2013) Induction of intestinal stem cells by R-spondin 1 and Slit2 augments chemoradioprotection. *Nature* 501:107–111.
36. Whangbo J, Kenyon C (1999) A Wnt signaling system that specifies two patterns of cell migration in *C. elegans*. *Mol Cell* 4:851–858.
37. Ghenea S, Boudreau JR, Lague NP, Chin-Sang ID (2005) The VAB-1 Eph receptor tyrosine kinase and SAX-3/Robo neuronal receptors function together during *C. elegans* embryonic morphogenesis. *Development* 132:3679–3690.
38. Fujisawa K, Wrana JL, Culotti JG (2007) The slit receptor EVA-1 coactivates a SAX-3/Robo mediated guidance signal in *C. elegans*. *Science* 317:1934–1938.
39. Watari-Goshima N, Ogura K, Wolf FW, Goshima Y, Garriga G (2007) *C. elegans* VAB-8 and UNC-73 regulate the SAX-3 receptor to direct cell and growth-cone migrations. *Nat Neurosci* 10:169–176.
40. Xu Y, Taru H, Jin Y, Quinn CC (2015) SYD-1C, UNC-40 (DCC) and SAX-3 (Robo) function interdependently to promote axon guidance by regulating the MIG-2 GTPase. *PLoS Genet* 11:e1005185.
41. Gao B, et al. (2011) Wnt signaling gradients establish planar cell polarity by inducing Vangl2 phosphorylation through Ror2. *Dev Cell* 20:163–176.
42. Yanfeng WA, et al. (2011) Functional dissection of phosphorylation of Disheveled in *Drosophila*. *Dev Biol* 360:132–142.
43. Gao C, Chen YG (2010) Dishevelled: The hub of Wnt signaling. *Cell Signal* 22:717–727.
44. Axelrod JD (2001) Unipolar membrane association of Dishevelled mediates Frizzled planar cell polarity signaling. *Genes Dev* 15:1182–1187.
45. Brenner (1974) The genetics of *Caenorhabditis elegans*. *Genetics* 77:71–94.